3D Printed Soft Skin for Safe Human-Robot Interaction

Joohyung Kim, Alex Alspach, and Katsu Yamane

Abstract— **The purpose of this research is the development of a soft skin module with a built-in airtight cavity in which air pressure can be sensed. A pressure feedback controller is implemented on a robotic system using this module for contact sensing and gentle grasping. The soft skin module is designed to meet size and safety criteria appropriate for a toy-sized interactive robot. All module prototypes are produced using a muti-material 3D printer. Experimental results from collision tests show that this module significantly reduces the impact forces due to collision. Also, using the measured pressure information from the module, the robotic system to which these modules are attached is capable of very gentle physical interaction with soft objects.**

I. INTRODUCTION

Humans interacting with robots in everyday environments is no longer just a subject of science fiction. Recently, Aldebaran's robot Pepper [1] has been working at stores greeting and interacting with customers in Japan. There are many service robots that dance, gesture and perform other functions to entertain, heal and educate people in places like amusement parks, hospitals and schools [2]–[6]. For more physically intimate interactions, such as carrying or hugging, it is imperative that these robots be soft and safe. For robots intended to interact with children or patients, these characteristics are important for preventing injuries and other accidents.

Over the last decade, researchers have studied soft robotics, utilizing the compliance and flexibility of soft materials to construct robots. Soft robots are often inspired by biology. Numerous biomimetic robots have been developed using soft materials such as a wall-climbing gecko [7] and crawling earthworms [8]. An important area of research in soft robotics is the development of safe robots and robotic devices that are designed for human interaction. Such robotic technologies have applications in the medical field [9] and in personal health care [10], to name only a couple. Biomimetic systems that combine the use of lightweight materials with passive, low-torque actuation have also been explored [11]. In soft robotics, the manufacturing and fabrication methods used to create soft sensors, actuators and structural components play a big role in obtaining the required characteristics for a given application [12]. These often complicated and delicate fabrication processes do not always produce parts with consistent quality and performance.

In conventional robotics, which deals with rigid components and precision actuators, there has also been considerable effort towards ensuring the safety of a human when interacting with a robot [13]–[18]. Most studies have focused on the prevention of collisions with humans or the use of sensor feedback control to reduce the impact when a collision does occur. Controllers for safe interaction can be designed in various ways depending on the capabilities of the robot and its ability to sense itself and its environment. A few examples which have been studied and applied for safe interaction are compliance control using joint torque sensors [13], impedance control using joint position [14] and tactile sensing control [15]. Further, some researchers [16]–[18] have studied the effects of collision during physical human-robot interaction (pHRI) using measures like the Head Injury Criterion (HIC) which is the likelihood of head injury due to a collision [19].

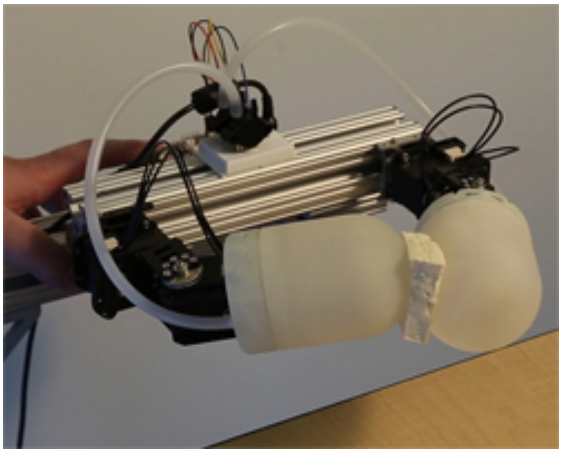

Fig. 1. Developed robotic system with 3D printed soft skin modules. The robot grasps a piece of tofu without crushing it. Our goal is to develop a robot that interact with children safely.

Our goal is to develop a toy-size robot that can physically interact with children. Existing toy-sized robots [4], [5] work well, perform various functions and are widely used in the academic field, but they must be watched carefully as to not hurt a child, nor be hurt by one. Because of their hard components and lack of integrated sensors, even a small movement of the robot can lead to an injury like a pinched finger. To achieve more safe and entertaining interaction, it is necessary to build a robot using soft materials with plenty of integrated sensors for control while still maintaining the functionalities of existing robots.

Here we present a 3D printed soft skin module with a built-in airtight cavity in which the air pressure can be sensed. A pressure feedback controller is implemented on a robotic system which uses this module for gentle grasping, as shown in Fig. 1. In the next section, we give and an

Joohyung Kim, Alex Alspach, and Katsu Yamane are with Disney Research, Pittsburgh, 4720 Forbes Ave., Suite 110, Pittsburgh, PA 15213, USA joohyung.kim@disneyresearch.com

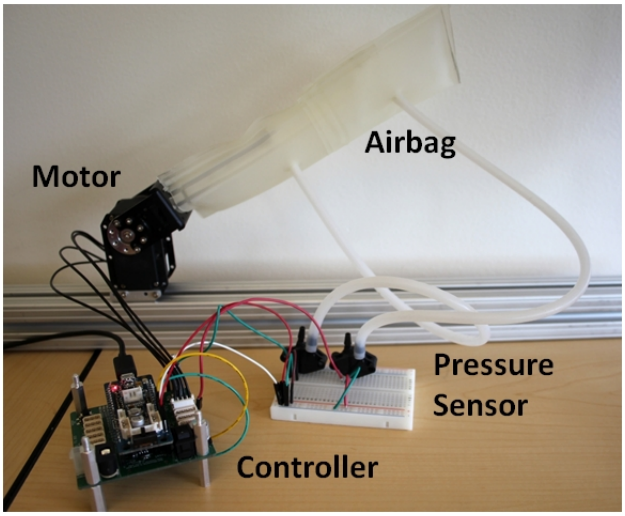

Fig. 2. Setup for pilot experiment. Pressurized airbags are connected to pressure sensors. Controller board receives the sensor values and sends control commands to the motor.

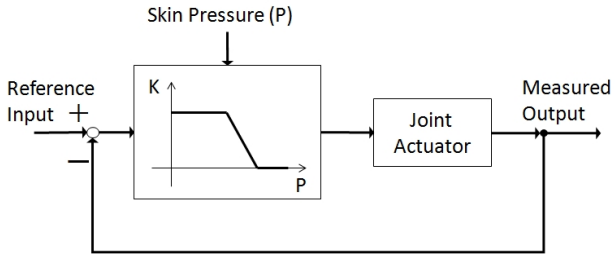

Fig. 3. Control framework for pilot experiment.

overview of our concept, including sensing methodologies and a control framework for safe interaction. We then discuss the design and fabrication of our proposed 3D soft skin module. In Sec. IV, we present experiments conducted to demonstrate the characteristics of the soft skin module and pressure feedback control. Conclusions and future work are discussed in Sec. V.

II. Concept Overview

An unexpected collision can cause a high peak force during a short period of contact. This impulsive force can lead to human injury and robot damage. Airbags are widely used as protective devices for reducing the impact force of a collision. Airbags are regarded as protective devices because they act as a mechanical low-pass filter when a collision occurs. In other words, an airbag may reduce the potential harm caused by a collision by decreasing the magnitude of the impact force and by increasing the overall duration of contact. To utilize this characteristic, we aim to cover the outside of a robot with air-filled components.

If the pressure in an airbag is greater than or equal to the pressure of the surrounding atmosphere, then the shape of the airbag will not change without the application of an external force. When contact is made between the airbag and the environment, the external force caused by this contact

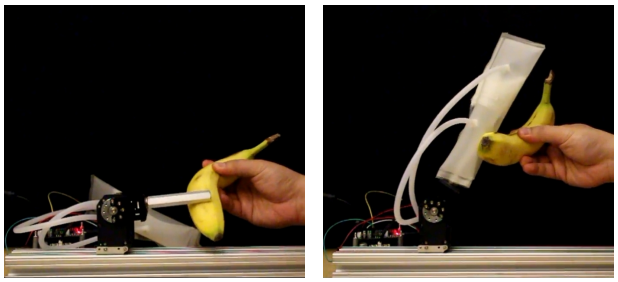

(a) Position control (b) Pressure feedback control

Fig. 4. Interaction with a soft object (banana). (a) Without an airbag and pressure feedback control, the banana was bent by the motor's rigid link. (b) Using the proposed pressure feedback control, the increase in airbag pressure due to contact decreased the motor torque and the banana was not bent.

may will deform the the airbag. Previous studies [10], [20] confirm that a pressure sensor can be used to sense a change in volume of a flexible airtight vessel. In this paper, we utilize the internal pressure information of the airbag for controlling the joints of a robot. Using an airbag that covers rigid links, like flesh over bone, a pressure feedback controller can be designed.

Figure 2 shows an experimental setup used to verify this concept. In the figure, each airbag is connected to a pressure sensor. These pressure sensors are connected to the A/D ports of the controller board which interfaces with the servo motor. There is a rigid link inside the airbag which connects to the motor axis, as shown in Fig. 4(a). The airbag is constructed using two rectangular polyurethane sheets which are bonded at the edges using an impulse heat-sealer. This airtight rectangular airbag is then rolled into a cylinderical shape as shown in Fig. 2. Each airbag is pressurized to hold its shape and connected to a pressure sensor using silicon tube. The pressure sensor in Fig. 2 is a MPX5500DP Freescale air pressure sensor. For the controller and actuator, we have selected ROBOTIS products which are widely used for robots with joint position controllers. Specifically, we use an MX-64T for the joint and an OpenCM9.04 microcontroller board with an OpenCM485EXP expansion board for the controller [21]. Position commands are sent to the servo every 10ms using TTL (Transistor-transistor Logic).

The proposed control system is depicted in Fig. 3. Using the Dynamixel MX-64T allows us to adjust the PID controller gains at every control step. In this system, we vary only the proportional gain,

$$u(t) = K_p(\theta_d(t) - \theta(t)), \tag{1}$$

where $u(t)$ is the control input to the joint, K_p is the proportional gain of the controller, and $\theta_d(t)$ and $\theta(t)$ are the desired and actual joint angles, respectively. The default proportional gain of Dynamixel servo controller is a constant. We use a function of the measured airbag pressure, $K(P(t))$,

as the proportional gain.

$$K(P(t)) = \begin{cases} K_p & \text{if } P(t) \leq P_{threshold} \\ K_p - aP(t) & \text{if } P_{threshold} < P(t) \leq P_{max} \\ 0 & \text{if } P_{max} < P(t) \end{cases},$$

$$\text{where } a = K_p/(P_{max} - P_{threshold}). \tag{2}$$

Here, K_p is the default proportional gain constant, $P_{threshold}$ is the pressure value at which the controller recognizes contact, and P_{max} is the pressure considered by the controller to be the maximum allowable pressure. As in Fig. 3 and Eq. (2), $K(P(t))$ becomes zero when the pressure is larger than P_{max} which results in the servo acting like a powerless joint.

This controller was implemented on the system in Fig. 2 to verify the feasibility of the proposed idea. For these pilot experiments, we set the desired motor trajectory to be a simple reciprocating motion from one joint extent to the other. In these experiments, the motion of the link was obstructed using a banana. Without the airbag, the rigid link tracks the given trajectory and continues to push on the banana after contact, deforming it as shown in Fig. 4(a). When using the airbag, the pressure feedback during contact reduces the motor torque, thereby reducing the force exerted on the banana as seen in Fig. 4(b).

Through these experiments, it was confirmed that using pressure information to sense contact and control joints is feasible. We also discovered that it is difficult to consistently fabricate airbags from polyurethane sheets using an impulse sealer.

III. 3D Printed Soft Skin

With recent advances in 3D printing, it is possible to create robot components with various material properties, from flexible to rigid, in a relatively short amount of time. To overcome the difficulties of producing polyurethane airbags, we leverage a multi-material 3D printer to fabricate a module with a rigid servo mount, soft outer skin and an airtight cavity. Since our goal is the development of a safe and interactive toy-sized robot for kids, the following components and design criteria are critical:

- Soft material for safe interaction and collision
- Airtight cavity for pressure sensing
- Size and shape able to be grasped by a child's hand
- Ability to rigidly attach to a servo motor

If a part is made of a soft material like rubber, it is hard to ensure a fixed connection with a rigid body. On the other hand, it is certain that a rigid and unyielding material is inadequate for soft and safe interaction. To achieve these conflicting design requirements, we print the single module using two materials simultaneously. The cross section of our design is depicted in Fig. 5. In the figure, the dark (blue) area is made of a rigid material and the light (yellow) area is made of a flexible material. The rigid end of the module is fixed to the motor using bolts. Also, a rigid link, analogous to a bone, extends within the air-filled cavity. The exterior of the module is made of flexible material which covers the rigid

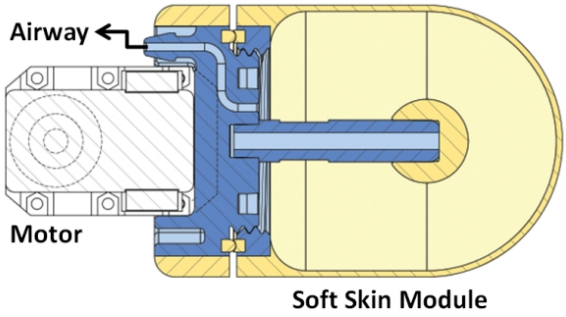

Fig. 5. Cross section of the 3D printed soft skin and motor. The dark (blue) area is made of a rigid material and the light (yellow) area is made of a flexible material

Fig. 6. 3D printed parts for soft skin module.

features and forms the airtight cavity in which the pressure is sensed. The module consists of three printed components, the base, the air-filled cavity and and the internal rigid link, as shown in Fig. 6. The base and air-filled cavity components are threaded for assembly. These two parts each contain a flexible O-ring-like mechanism that deforms against the other when assembled to create an airtight seal. Once assembled, air can go in and out only through the airway shown in Fig. 5. This airway is terminated with a barbed tube fitting for easy connection with standard silicone tubing. The rigid link within the cavity has a soft ball at the end to protect the interior of the air-filled cavity. All components were designed in SolidWorks and printed using VeroWhitePlus (rigid material) and TangoPlus (flexible material) on an Objet Eden 260V 3D printer [22].

The outer diameters of the cylindrical and hemispherical features are 65mm and the length from the motor axis to the opposite tip of the module is 121.26mm. The diameter of the internal rigid link is 10mm with a length of 40mm. The ball at the tip of this link is 20mm in diameter. The thickness of the material surrounding the air-filled cavity is 1.5mm. The total volume of cavity is about 173cm^3.

This soft skin module is connected to the pressure sensor using a silicon tube. For experimental repeatability when testing multiple modules, the modules are not pressurized, but instead tested with the air-filled cavity at atmospheric pressure. The proposed 3D printed module outputs sensitive pressure data up to about 5psi and has enough flexibility when sealed to be compressed until the internal rigid link is felt through the skin.

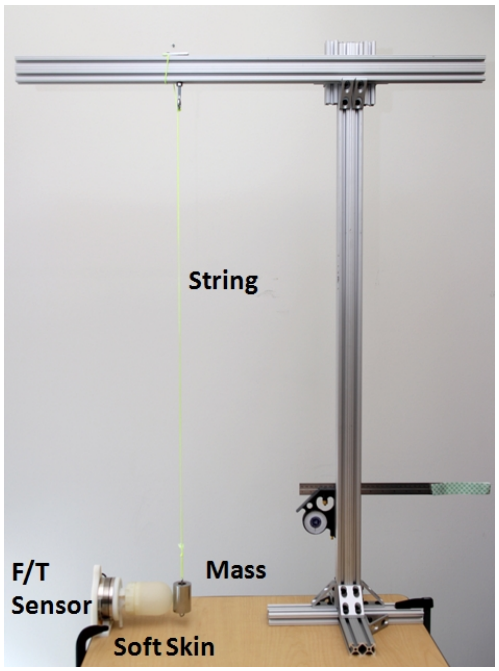

Fig. 7. Experimental setup for collision test.

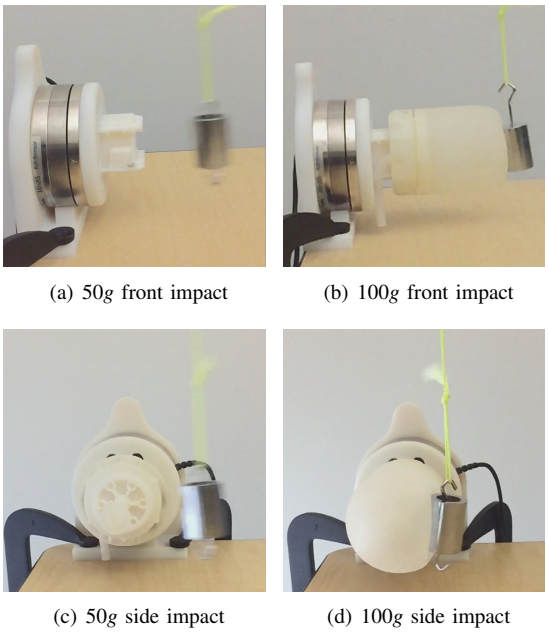

(a) 50g front impact (b) 100g front impact

(c) 50g side impact (d) 100g side impact

Fig. 8. Four collision test cases

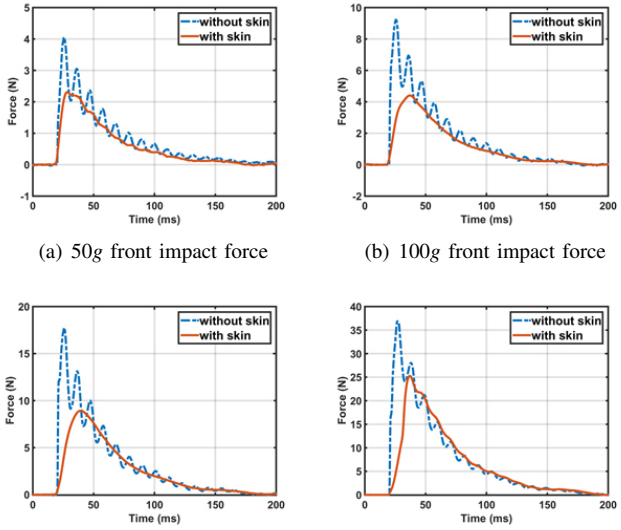

(a) 50g front impact force (b) 100g front impact force

(c) 200g front impact force (d) 500g front impact force

Fig. 9. Front impact results with and without soft skin module.

IV. Experiment

In this section, we present our setup and results for multiple experiments conducted to show the characteristics of the proposed 3D printed soft skin module and pressure feedback control.

A. Collision Test

As mentioned in the previous sections, the peak magnitude of the collision force and the time from initial impact to this peak force are important factors when concerned with safety. To measure the effect of an external impact on a robot, we developed the experimental setup shown Fig. 7. The structure on the right of the figure supports a hanging pendulum. The 3D printed soft skin module is located opposite this structure where it is mounted to a 6-axis force/torque sensor. The 3D printed rigid fixture used to attach the soft skin module to the force/torque sensor shares the overall form and mounting geometry of a MX-64T servo with its output axis and geometric center aligned with the sensing origin of the force/torque sensor.

The impact experiments are conducted by releasing the pendulum mass at rest (m) from a constant height (h) so that it hits the link at the lowest point of its trajectory. The length of the pendulum, from the pivot axis to the center of mass, is 1m and the height (h) from which the mass is released is 0.2m. We performed four sets of experiments varying the direction of the impact with and without the soft skin module attached. In the case of the pendulum impacting the front of the link without the soft skin module (Fig. 8(a)), only the servo-shaped fixture is attached to the force/torque sensor in order to measure the impact of rigid body collision with the link. Figure 8(b) shows the case where the pendulum hits the front of the link with the soft skin module attached. In Figs. 8(c) and 8(d), side impact experiments are shown. In Fig. 8(c), the base and internal link of the soft skin module are attached to the force/torque sensor in order to keep the distance between the impact point and the force/torque sensing origin congruent with that of Fig. 8(d). For each of these experiments, we use 4 different pendulum masses (m), 50g, 100g, 200g and 500g.

The results from the front impact experiments are depicted in Fig. 9 and the results from the side impact experiments are in Fig. 10. In the case of the front impact experiments, all of the obtained force and torque values from the sensor are negligible except for the force in the direction of impact, which is F_Z in the sensor's coordinate frame. In the side

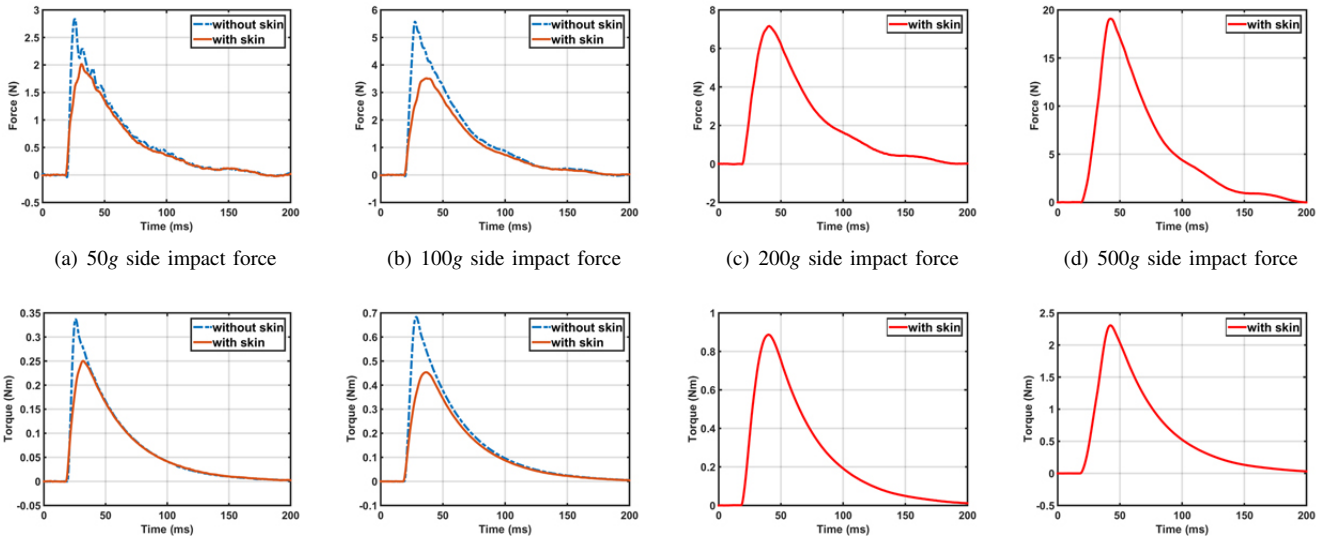

(a) 50g side impact force (b) 100g side impact force (c) 200g side impact force (d) 500g side impact force

(e) 50g side impact torque (f) 100g side impact torque (g) 200g side impact torque (h) 500g side impact torque

Fig. 10. Side impact results with and without soft skin module.

TABLE I

FRONT IMPACT FORCE RESULTS

soft skin	mass (g)	50	100	200	500
without	peak force (N)	4.054	9.241	17.737	36.889
	time to peak (ms)	5.857	5.857	6.000	7.000
with	peak force (N)	2.315	4.412	8.929	25.275
	time to peak (ms)	8.286	17.143	20.000	17.000

TABLE II

SIDE IMPACT FORCE AND TORQUE RESULTS

soft skin	mass (g)	50	100	200	500
without	peak force (N)	2.841	5.575	N/A	N/A
	peak torque (Nm)	0.337	0.683	N/A	N/A
	time to peak (ms)	8.714	5.857	N/A	N/A
with	peak force (N)	2.024	3.513	7.161	19.087
	peak torque (Nm)	0.250	0.457	0.887	2.306
	time to peak (ms)	16.428	17.143	20.143	22.571

impact experiments, the force in the impact direction (F_Y) and corresponding torque (T_X) values are dominant. Each of the graphs in the figures show the average of 10 sets of experimental results. The solid (red) lines are the results of impact with the 3D printed soft skin module, and the dotted lines (blue) are the results without the soft skin module. In Fig. 10, there are no dotted lines in the graphs for the 200g and 500g mass impacts because the module's internal link could not withstand the impact, breaking during the 200g mass experiments. Each graph shows that the peak value of the solid line is smaller in magnitude than the peak value of the dotted line and that the time to peak of the solid line is later than that of the dotted line. More specifically, in the front impact experiments with the soft skin module attached, the peak force was decreased by 32-52% and the time between initial impact and peak force is 1.4-3.3 times longer. In the side impact experiments, it was verified that the soft skin reduced the peak force and torque by 26-37% and increased the time to peak by 1.9-2.9 times. The average peak force and time to peak in each case are denoted in Tables I and II.

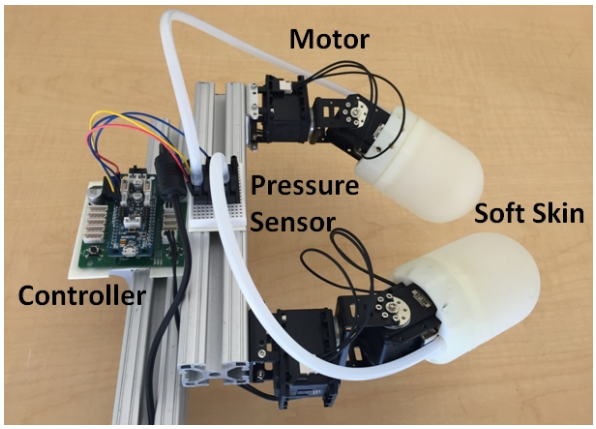

Fig. 11. 4 DoF grasping robot with soft skin modules.

B. Grasping Test

In this section, we present grasping experiments using a four degree-of-freedom robotic system. The goal of these experiments is to characterize the sensitivity of our soft skin module and the ability to control a system using it.

The robotic system for grasping is shown in Fig. 11. Each limb consists of two MX-64T servo motors with a 3D printed soft skin module attached at the end. The servo motors adjacent to the skin modules rotate inwards for grasping objects while the other two motors rotate the grasping joints to move objects in the vertical direction. The controller board and pressure sensors are the same as in the pilot experiment. The robotic system's active and gentle interaction with a

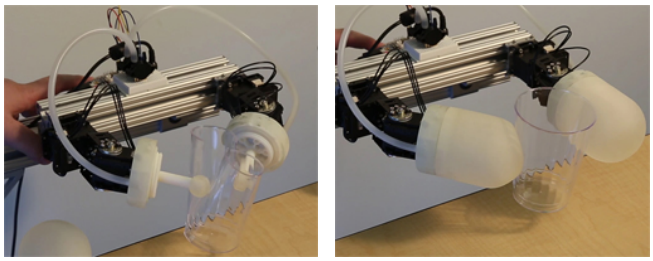

(a) Plastic cup without soft skin (b) Plastic cup with soft skin

(c) Aluminum can with soft skin (d) Roll of paper with soft skin

Fig. 12. Grasping experiments

grasped object extends to its ability to safely interact with its environment.

A trajectory modification controller is implemented based on the pressure information from the soft skin modules. The controller for the grasping joint angle ($\theta_d^G(k)$) is described as

$$\theta_d^G(k) = \begin{cases} \theta_d^G(k-1) - a & \text{if } P(k) \leq P_c \\ \theta_d^G(k-1) & \text{if } P_c < P(k) \leq P_p \\ \theta_d^G(k-1) + b & \text{if } P_p < P(k) \end{cases}, \quad (3)$$

$$\text{where } \theta_{min} \leq \theta_d^G(k) \leq \theta_{max}.$$

In Eq. (3), $P(k)$ is the sensed pressure, a and b are the inward and outward velocities, and θ_{min} and θ_{max} are the minimum and maximum angles of the grasping joint. Once the grasping motion is commanded, $\theta_d^G(k)$ begins moving inward. If the pressure of either module exceeds P_c, the grasping joint on that side maintains its angle. If the pressure exceeds P_p, then the grasping joint rotates outward. Using this simple control scheme, the limbs compete with each other to keep their pressure values within a certain range and effectively hold an object between the soft skin modules. The two lifting joints are moved symmetrically upward and downward on command, regardless of the pressure sensor readings.

This grasping controller was tested using several objects. Without the soft skin for pressure feedback, the servo motors track the desired trajectories and generate a torque strong enough to crush a disposable plastic cup using the exposed internal links of the modules as shown in Fig. 12(a). In Fig. 12(b), the same kind of plastic cup is used with the soft skin modules attached and the grasping control described in Eq. (3). In this experiment, the cup is not crushed, but instead gently held. While grasping, it is possible to move the cup by hand while the robot follows and maintains contact. This system is also able to grasp an aluminum can, a roll of letter size printer paper and a piece of tofu without crushing any, as shown in Figs. 1, 12(c) and 12(d). In all cases seen in in Figs. 1 and 12, we use fixed threshold pressure values to recognize contact (P_c) and larger external forces like that of pushing on the grasped object (P_p).

V. Conclusion and Future Work

A soft skin module with a built-in airtight cavity for sensing air pressure is presented. This module is integrated into a robotic system with pressure feedback control to enable safe physical interaction. The soft skin module is designed to meet size and safety criteria appropriate for a toy-sized robot. All module prototyping is done using muti-material 3D printing. Collision test results show that this module reduces the impact of collision on the robot. Further, using the measured pressure information from the modules, a robotic system capable of very gentle physical interaction with soft objects is demonstrated.

We plan to continue searching for proper methods of analyzing the effects of collision in small robots. Although the HIC has been widely used in the robotics field, it is not an appropriate metric for evaluating the collisions experienced by toy robots, which are very small compared to those of industrial robots or vehicle collisions as mentioned in [18]. The design concept of the 3D printed soft skin module presented in this paper will be used to make other modules of varying geometry in the future. This expansion of the concept and application will allow us to integrate the soft skin modules into our previous research [23] , which is the implementation of a walking biped robot that resembles an animated character both physically and in its actions.

References

[1] Aldebaran. (2014) Who is pepper? [Online]. Available: www.aldebaran.com/en/a-robots/who-is-pepper

[2] Y. Sakagami, R. Watanabe, C. Aoyama, S. Matsunaga, N. Higaki, and K. Fujimura, "The intelligent asimo: System overview and integration," in *Intelligent Robots and Systems, 2002. IEEE/RSJ International Conference on*, vol. 3. IEEE, 2002, pp. 2478–2483.

[3] M. Fujita, Y. Kuroki, T. Ishida, and T. Doi, "Autonomous behavior control architecture of entertainment humanoid robot sdr-4x," in *Intelligent Robots and Systems, 2003. (IROS 2003). Proceedings. 2003 IEEE/RSJ International Conference on*, vol. 1, Oct 2003, pp. 960–967 vol.1.

[4] I. Ha, Y. Tamura, H. Asama, J. Han, and D. W. Hong, "Development of open humanoid platform darwin-op," in *SICE Annual Conference (SICE), 2011 Proceedings of*. IEEE, 2011, pp. 2178–2181.

[5] Aldebaran. (2014) Who is nao? [Online]. Available: https://www.aldebaran.com/en/humanoid-robot/nao-robot

[6] K. Wada, T. Shibata, T. Musha, and S. Kimura, "Robot therapy for elders affected by dementia," *Engineering in Medicine and Biology Magazine, IEEE*, vol. 27, no. 4, pp. 53–60, July 2008.

[7] S. Kim, M. Spenko, S. Trujillo, B. Heyneman, V. Mattoli, and M. Cutkosky, "Whole body adhesion: hierarchical, directional and distributed control of adhesive forces for a climbing robot," in *Robotics and Automation, 2007 IEEE International Conference on*, April 2007, pp. 1268–1273.

[8] A. Menciassi, S. Gorini, G. Pernorio, L. Weiting, F. Valvo, and P. Dario, "Design, fabrication and performances of a biomimetic robotic earthworm," in *Robotics and Biomimetics, 2004. ROBIO 2004. IEEE International Conference on*, Aug 2004, pp. 274–278.

[9] Y.-L. Park, B. rong Chen, N. O. Prez-Arancibia, D. Young, L. Stirling, R. J. Wood, E. C. Goldfield, and R. Nagpal, "Design and control of a bio-inspired soft wearable robotic device for anklefoot rehabilitation," *Bioinspiration & Biomimetics*, vol. 9, no. 1, p. 016007, 2014. [Online]. Available: http://stacks.iop.org/1748-3190/9/i=1/a=016007

[10] S. Sanan, M. Ornstein, and C. Atkeson, "Physical human interaction for an inflatable manipulator," in *Engineering in Medicine and Biology Society, EMBC, 2011 Annual International Conference of the IEEE*, Aug 2011, pp. 7401–7404.

[11] J. Whitney and J. Hodgins, "A passively safe and gravity-counterbalanced anthropomorphic robot arm," in *Robotics and Automation (ICRA), 2014 IEEE International Conference on*, May 2014, pp. 6168–6173.

[12] K.-J. Cho, J.-S. Koh, S. Kim, W.-S. Chu, Y. Hong, and S.-H. Ahn, "Review of manufacturing processes for soft biomimetic robots," *International Journal of Precision Engineering and Manufacturing*, vol. 10, no. 3, pp. 171–181, 2009. [Online]. Available: http://dx.doi.org/10.1007/s12541-009-0064-6

[13] J. Kim, Y. Lee, S. Kwon, K. Seo, H. Kwak, H. Lee, and K. Roh, "Development of the lower limbs for a humanoid robot," in *Intelligent Robots and Systems (IROS), 2012 IEEE/RSJ International Conference on*. IEEE, 2012, pp. 4000–4005.

[14] A. Albu-Schaffer, O. Eiberger, M. Grebenstein, S. Haddadin, C. Ott, T. Wimbock, S. Wolf, and G. Hirzinger, "Soft robotics," *Robotics Automation Magazine, IEEE*, vol. 15, no. 3, pp. 20–30, September 2008.

[15] R. Dahiya, G. Metta, M. Valle, and G. Sandini, "Tactile sensing;from humans to humanoids," *Robotics, IEEE Transactions on*, vol. 26, no. 1, pp. 1–20, Feb 2010.

[16] S. Haddadin, A. Albu-Schaffer, M. Frommberger, J. Rossmann, and G. Hirzinger, "The dlr crash report: Towards a standard crash-testing protocol for robot safety - part i: Results," in *Robotics and Automation, 2009. ICRA '09. IEEE International Conference on*, May 2009, pp. 272–279.

[17] S. Haddadin, A. Albu-Schaffer, M. Frommberger, J. Rossmann, and G. Hirzinger, "The dlr crash report: Towards a standard crash-testing protocol for robot safety - part ii: Discussions," in *Robotics and Automation, 2009. ICRA '09. IEEE International Conference on*, May 2009, pp. 280–287.

[18] J.-J. Park, S. Haddadin, J.-B. Song, and A. Albu-Schaffer, "Designing optimally safe robot surface properties for minimizing the stress characteristics of human-robot collisions," in *Robotics and Automation (ICRA), 2011 IEEE International Conference on*, May 2011, pp. 5413–5420.

[19] J. Versace, "A review of the severity index," SAE Technical Paper, Tech. Rep., 1971.

[20] R. Slyper and J. Hodgins, "Prototyping robot appearance, movement, and interactions using flexible 3d printing and air pressure sensors," in *RO-MAN, 2012 IEEE*, Sept 2012, pp. 6–11.

[21] Robotis. (2014) Mx-106 e-manual. [Online]. Available: http://http://support.robotis.com/en/home.htm

[22] Stratasys. (2014) Object260 connex. [Online]. Available: http://www.stratasys.com/3d-printers/design-series/objet260-connex

[23] S. Song, J. Kim, and K. Yamane, "Development of a bipedal robot that walks like an animation character," in *Robotics and Automation, 2015. ICRA '15. IEEE International Conference on*, accepted.